Influence of thermal strains on the electrocaloric and dielectric properties of ferroelectric nanoshells

Xiao Dai,[1] Hai-Xia Cao,[1,a)] Qing Jiang,[1] and Veng Cheong Lo[2]
[1]*Department of Physics and Jiangsu Key Laboratory of Thin Films, Soochow University, Suzhou 215006, China*
[2]*Department of Applied Physics, The Hong Kong Polytechnic University, Hong Kong, China*

(Received 6 May 2009; accepted 27 June 2009; published online 3 August 2009)

The electrocaloric effect and dielectric tunability of $BaTiO_3$ ferroelectric nanoshells on Si and MgO cores are investigated using the modified Landau–Ginzburg–Devonshire theory, in which the surface tension and thermal strain are taken into account. The numerical results exhibit a peak of electrocaloric coefficient near the critical nanoshell thickness accompanied with the size-driven phase transition. In addition to the enhanced adiabatic temperature difference, the compressive thermal strain also significantly improves the dielectric tunability. More importantly, the ferroelectric nanoshell displays pronounced electrocaloric effect: $\Delta T(T_m)=2.09$ K for the nanoshell on Si core and $\Delta T(T_m)=2.33$ K on MgO core, respectively. Essentially, the ferroelectric nanoshell provides an effective means to acquire good electrocaloric effect and high dielectric tunability by adjusting the wall thickness, core radius, annealing temperature, and various core materials, which may effectively contribute to the stress level in the ferroelectric nanoshell. © *2009 American Institute of Physics*. [DOI: 10.1063/1.3186057]

I. INTRODUCTION

Ferroelectric materials have drawn considerable attention due to their applications in micro- and nanoelectronic devices such as sensors, microactuators, infrared detectors, microwave phase filters, nonvolatile memories, and tunable dielectric devices. In particular, recent advances in the synthesis and fabrication of micro- and nanoscale ferroelectric structures[1,2] have revealed that further study need to be conducted to understand the new physical phenomena in this size range. Nowadays, various ferroelectric nanostructures—ultrathin films,[3] nanowires,[4] nanotubes,[5,6] nanoislands,[7] nanorings,[8] and nanocells[9]—can be grown with control at the atomic scale. With the decrease in the ferroelectric size, the size-dependent ferroelectric behaviors and their possible disappearance at critical size become crucial.[10–12] Many theoretical[13–16] and experimental researches[17–19] have demonstrated that the phase transformation, dielectric, piezoelectric, and pyroelectric properties are dramatically different from those observed in bulk ceramics or crystals. These new features can be attributed to the intrinsic size effect, surface tension, and the electromechanical coupling between the spontaneous polarization and the internal stress field of the ferroelectric nanostructures. Most researchers are focusing on the critical behavior, and dielectric and piezoelectric responses; nevertheless, not much work has been done on the electrocaloric effect (ECE) of the ferroelectric nanostructures.

The ECE occurs when an electric field changes the temperature of a polarizable material under reversible and adiabatic conditions. The ECE may provide an efficient means to realize solid-state cooling devices for a broad range of applications such as on-chip cooling and temperature regulation for sensors and electronic devices, provided that materials with large ECE can be developed. Refrigeration based on the ECE approach is more environmental friendly and hence may also provide an alternative to the existing vapor-compression approach. The ferroelectric material is an excellent representative exhibiting a large ECE in that it generates a large entropy change associated with the polarization change. The recent discovery of a large ECE in thin film $PbZr_{0.95}Ti_{0.05}O_3$ (Ref. 20) and relaxor ferroelectric $0.9PbMg_{1/3}Nb_{2/3}O_3$-$0.1PbTiO_3$ (0.9PMN-0.1PT) (Ref. 21) has stimulated several experimental and theoretical studies with regard to this subject. Neese *et al.*[22] demonstrated that a large ECE can be achieved in the ferroelectric poly(vinylidene fluoride-trifluoroethylene) copolymer at temperatures above the ferroelectric-paraelectric transition, where an isothermal entropy change of more than 55 J/kg K and adiabatic temperature change ΔT of more than 12 °C were observed. Hagberg *et al.*[23] reported that the existence of two electrocaloric maxima in reactive sintered relaxor ferroelectric 0.87PMN-0.13PT was an indication of several mechanisms responsible for the ECE. Furthermore, Akcay *et al.*[24,25] studied the intrinsic ECE in bulk and thin film $BaTiO_3$ using a thermodynamic theory. Their work implies that the control of misfit strain by appropriate choice of substrate provides a potential means to alter both the magnitude and the temperature sensitivity of the ECE. Dunne *et al.*[26] introduced a microscopic theory of the ECE in the paraelectric phase of potassium dihydrogen phosphate KH_2PO_4 based on Slater's lattice model and gave a remarkably accurate description of the electric field dependence of the ECE. Recently first-principles-derived effective Hamiltonians and nonequilibrium molecular dynamics have been combined to compute ECE directly in a cubic nanodot $Pb(Zr_{0.4}Ti_{0.6})O_3$, which ex-

a)Author to whom correspondence should be addressed. Electronic mail: hxcao@suda.edu.cn.

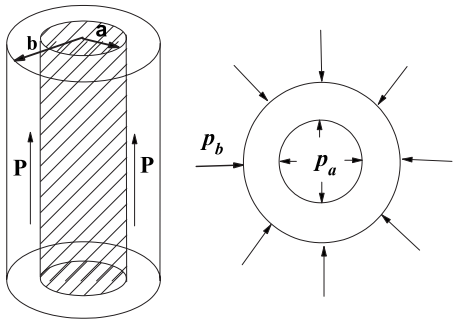

FIG. 1. Schematic diagrams of a nanoshell on cylindrical core.

hibited an unusual field-induced change in temperature.[27] Obviously, most of the work on the ECE concentrated on the ferroelectric bulk and thin films. The ECE of ferroelectric nanostructures has not been fully investigated.

In this paper, a modified Landau–Ginzburg–Devonshire (LGD) thermodynamic theory is used to study the impact of thermal strains on the ECE and dielectric properties of ferroelectric nanoshells. Investigations have shown that the internal strains play an important role in the ECE properties of $BaTiO_3$ film.[25] Internal stresses usually arise from the lattice mismatch between the film and substrate for epitaxial grown films, the difference in thermal expansion coefficients (TECs) of the film and the substrate, the surface curvature in the nanostructures, defects such as dislocations and vacancies, and the self-strain of the ferroelectric phase transition for the material grown above the phase transition temperature. Although the influence of surface tension and size effect on the phase diagrams and polar properties of ferroelectric nanowires and nanotubes have been fully discussed based on the LGD theory,[10,14,28] the impact of the internal thermal strains on the ECE properties and dielectric properties of nanoshells have not been reported yet. We believe a deep understanding of the relationship between the thermal strains and ECE, as well as the dielectric response in ferroelectric nanoshells, will provide guidelines on how to improve the dielectric tunability, electrocaloric coefficient, and adiabatic temperature change by manipulating the thermal stress level. This might be crucial for application of ferroelectric nanostructures.

II. THEORETICAL DEVELOPMENT

We consider a $BaTiO_3$ ferroelectric nanoshell on a cylindrical core, with an inner radius (IR) a and outer radius b, as shown in Fig. 1. A cylindrical coordinate is established and the z axis coincides with the cylindrical axis of the nanoshell. The polarization P is aligned axisymmetrically along the [001] axis direction, i.e., $P(r)=P[0,0,P(z)]$. Based on the LGD theory, the total free energy per unit length of the ferroelectric nanoshell is given by[14]

$$G = G_0 + G_V + G_S = G_0 + \int_a^b 2\pi r dr \left\{ a_{1\sigma} P^2(r) + a_{11} P^4(r) + a_{111} P^6(r) + \frac{1}{2} K \left[\frac{\partial P(r)}{\partial r} \right]^2 - E_0 P \right\} + K\delta^{-1}\pi [aP^2(r=a) + bP^2(r=b)], \quad (1)$$

where $a_{1\sigma}$, a_{11}, and a_{111} are the modified dielectric stiffness and higher-order dielectric stiffness coefficients, respectively. K, δ, and E_0 represent the gradient energy coefficient, extrapolation length, and external electric field, respectively. Then the following Euler–Lagrange equation can be obtained using direct variational approach:

$$K\left(\frac{d^2P}{dr^2} + \frac{1}{r}\frac{dP}{dr} \right) - 2a_{1\sigma}P - 4a_{11}P^3 - 6a_{111}P^5 - E_0 = 0, \quad (2)$$

with the boundary conditions

$$\frac{dP}{dr} = \frac{P}{\delta}, \quad r=a, \quad \frac{dP}{dr} = -\frac{P}{\delta}, \quad r=b. \quad (3)$$

Considering the stress effect, the coefficient $a_{1\sigma}$ should be renormalized:

$$a_{1\sigma} = a_1(T - T_C) - Q_{12}(\sigma_{rr} + \sigma_{\varphi\varphi}) - Q_{11}\sigma_{zz}, \quad (4)$$

where σ_{rr}, $\sigma_{\varphi\varphi}$, and σ_{zz} are the radial, tangential, and axial components of the stress field in the nanoshell, respectively.

In our calculation, both the surface tension induced strain and the thermal strain have been taken into consideration. Under radial pressures p_a and p_b at the inner and outer surfaces, as shown in Fig. 1, the surface tension induced strain can be expressed as[29]

$$\sigma_{rr}(r) = \frac{a^2b^2}{b^2-a^2}\frac{p_b - p_a}{r^2} + \frac{a^2p_a - b^2p_b}{b^2-a^2},$$

$$\sigma_{\varphi\varphi}(r) = -\frac{a^2b^2}{b^2-a^2}\frac{p_b - p_a}{r^2} + \frac{a^2p_a - b^2p_b}{b^2-a^2}. \quad (5)$$

For the nanoshell, $p_a=-u_a/a$ and $p_b=-u_b/b$ in Eq. (5) are the radial stresses, where u_a and u_b are the inner and outer surface energy densities, respectively. Assuming $u_a=u_b=u$, we then have

$$\sigma_{rr} + \sigma_{\varphi\varphi} \approx -\frac{u}{b-a}\exp\left(-\frac{R_C}{b-a} \right), \quad (6)$$

where R_C is the characteristic thickness of a nanoshell.[28] The expression in Eq. (6) avoids the unphysical divergence when the thickness of the nanoshell reduces to zero. On the other hand, the temperature field can be regarded as uniform throughout the nanoshell. According to the elasticity theory, the stress-strain equations in cylindrical coordinate system can be expressed as

$$\varepsilon_r = \frac{1}{M}[\sigma_r - \nu(\sigma_\varphi + \sigma_z)] + \alpha\Delta T',$$

$$\varepsilon_\varphi = \frac{1}{M}[\sigma_\varphi - \nu(\sigma_r + \sigma_z)] + \alpha\Delta T',$$

$$\varepsilon_z = \frac{1}{M}[\sigma_z - \nu(\sigma_r + \sigma_\varphi)] + \alpha\Delta T', \quad (7)$$

where $\varepsilon_{r(\varphi,z)}$, $\sigma_{r(\varphi,z)}$, and υ correspond to the strain, stress, and Poisson's ratio, respectively. M denotes the elastic modulus and α represents TEC, and $\Delta T' = T - T_A$ is the dif-

ference between the ambient temperature and annealing temperature. The thermal strain in the ferroelectric nanoshells originates from the deposition temperature or from the annealing temperature depending on the deposition process. The reference temperature that determines the thermal strain relies on what is chosen as the processing technique. For chemical deposition techniques such as spin coating or metal organic chemical vapor deposition, the critical temperature is the one at which the final annealing is carried out. For physical vapor deposition methods such as pulsed laser deposition, the temperature of interest is the one of the substrate at which the deposition is carried out. Here we only concentrate on the thermal strain arising from the annealing temperature. The annealing at high temperatures will not only increase the crystallinity but also change the boundary conditions with the formation of interfacial layer; thus it could probably be a shortcut to adjust the ECE and dielectric response of nanoshells through thermal strain. Assuming that the thermal induced radial pressure at the interface is p', we get the stress-strain relations shown in Eqs. (8) for the core and in Eq. (9) at the interface $r=a$ between the core and the shell combining Eq. (5) with Eq. (7):

$$\sigma_r' = \sigma_\varphi' = -p',$$

$$\varepsilon_r' = \frac{1}{M'}[-p - \nu'(-p' + \sigma_z')] + \alpha'\Delta T',$$

$$\varepsilon_\varphi' = \frac{1}{M'}[-p - \nu'(-p' + \sigma_z')] + \alpha'\Delta T',$$

$$\varepsilon_z' = \frac{1}{M'}[\sigma_z' - \nu'(-p' - p)] + \alpha'\Delta T', \tag{8}$$

$$\sigma_r = -p', \quad \sigma_\varphi = \frac{b^2 + a^2}{b^2 - a^2}p',$$

$$\varepsilon_r = \frac{1}{M}\left[-p' - \nu\left(\frac{b^2 + a^2}{b^2 - a^2}p' + \sigma_z\right)\right] - \alpha\Delta T',$$

$$\varepsilon_\varphi = \frac{1}{M}\left[\frac{b^2 + a^2}{b^2 - a^2}p' - \nu(-p' + \sigma_z)\right] + \alpha\Delta T',$$

$$\varepsilon_z = \frac{1}{M}\left[\sigma_z - \nu\left(-p' + \frac{b^2 + a^2}{b^2 - a^2}p'\right)\right] + \alpha\Delta T', \tag{9}$$

with the boundary conditions

$$-\varepsilon_r = \varepsilon_r',$$

$$\varepsilon_\varphi = \varepsilon_\varphi{}',$$

$$\varepsilon_z = \varepsilon_z{}'. \tag{10}$$

By solving the set of Eqs. (8)–(10), the radial, tangential, and axial components of the stress field in the nanoshell can be expressed as follows:

$$p' = \frac{\Delta T' MM'(b^2 - a^2)(1 + \nu')(\alpha' - \alpha)}{(b^2 - a^2)[E'(1 + \nu) + E(1 + \nu')(1 - 2\nu')] + a^2E'[2(1 - \nu\nu') + (\nu'/\nu - 1)(1 - \nu)]},$$

$$\sigma_z = \frac{a^2(1 - \nu)}{\nu(b^2 - a^2)}p',$$

$$\sigma_r + \sigma_\varphi = \frac{2a^2}{b^2 - a^2}p'. \tag{11}$$

Based on Eqs. (4), (6), and (11), the dielectric stiffness coefficient $a_{1\sigma}$ can then be deduced as

$$a_{1\sigma} = a_1(T - T_{C0}) - Q_{12}\left[\frac{2a^2}{b^2 - a^2}p' - \frac{u}{b - a}\exp\left(-\frac{R_C}{b - a}\right)\right] - Q_{11}\frac{a^2(1 - \nu)}{\nu(b^2 - a^2)}p'. \tag{12}$$

As a result, the role of the surface tension and thermal strain effect of the substrate can be determined from the above modified dielectric stiffness coefficient.

The equilibrium polarization P^0 of the shell is numerically calculated from Eq. (2). According to the thermodynamic theory, the excess entropy S^{XS} and the excess specific heat $\Delta C_{E,\sigma}$ of the ferroelectric nanoshell, under constant applied electric field and stress, can be expressed as

$$S_{E,\sigma}^{XS} = -\left(\frac{\partial G}{\partial T}\right)_{E,\sigma}, \tag{13}$$

$$\Delta C_{E,\sigma} = -T\left(\frac{\partial^2 G}{\partial T^2}\right)_{E,\sigma}. \tag{14}$$

The electrocaloric coefficient is defined by

$$p = \left(\frac{\partial P^0}{\partial T}\right)_{E,\sigma} = \left(\frac{\partial S}{\partial E}\right)_{T,\sigma}. \tag{15}$$

By computing the values of $\Delta C_{E,\sigma}$ and P^0 as functions of T, E, and $\varepsilon_{r(\varphi,z)}$, the temperature change induced by the variation in applied electric field at adiabatic condition can be determined through

TABLE I. TEC, elastic modulus, and Poisson's ratio of $BaTiO_3$, Si, and MgO.

	$BaTiO_3$	Si	MgO
TEC (10^{-6} mm/mm °C)	10.6	2.6	13.5
Elastic modulus (GPa)	148	169	187
Poisson's ratio	0.3	0.358	0.18

$$\Delta T = -T\int_{E_1}^{E_2} \frac{1}{C_{E,\sigma}}\left(\frac{\partial P^0}{\partial T}\right)_{E,\sigma} dE. \tag{16}$$

Here the absolute value of the heat capacity $C_{E,\sigma}$ can be estimated by scaling the computed zero-field values of the excess specific heat $\Delta C_{E,\sigma}$ given in Eq. (14) to the lattice contributions extracted from the experimental values.[25] $E_2 - E_1 = \Delta E$ is the difference in the applied electric field. In addition, the dielectric constant of ferroelectric nanoshell is determined from

$$\varepsilon = \frac{1}{\varepsilon_0}\frac{\partial P^0}{\partial E}. \tag{17}$$

Correspondingly, the dielectric tunability Φ is defined as the relative change in the dielectric constant at a certain external field $\varepsilon(E)$ with respect to the value at zero field $\varepsilon(0)$ as follows:

$$\Phi = \frac{\varepsilon(0) - \varepsilon(E)}{\varepsilon(0)} \times 100\%. \tag{18}$$

III. RESULTS AND DISCUSSION

Various substrates, which provide different thermal expansion induced strain, can be employed to study the strain dependence of electrocaloric properties and dielectric response because the boundary conditions imposed by a core profoundly affect ferroelectricity in the ferroelectric nanoshells. In our calculation, we consider FE nanoshells on two different cylindrical cores: one is Si, and the other is MgO. TEC of $BaTiO_3$ is greater than that of Si; consequently, the tensile thermal strain in the nanoshell on Si core may be built up while cooling down from the annealing temperature. On the contrary, the compressive thermal strain exists for the nanoshell on MgO core since the TEC of $BaTiO_3$ is less than that of MgO. TECs, elastic modulus, and Poisson's ratios of $BaTiO_3$, Si, and MgO used in this study are given in Table I.

First, we investigate the impact of the wall thickness, IR, and annealing temperature on the electrocaloric coefficient. Figure 2 shows the electrocaloric coefficient as a function of the wall thickness of nanoshell on MgO and Si cores for the various nanoshell IRs, at room temperature $T=300$ K and annealing temperature $T_A=900$ K. It is discovered that nanoshell on MgO exhibits a larger electrocaloric coefficient than that on Si, irrespective of the wall thickness and IR. This means the compressive thermal strain is of great benefit to the electrocaloric coefficient. Besides, the electrocaloric coefficient is not a monotonous function of the nanoshell wall thickness, and a peak of electrocaloric coefficient exists

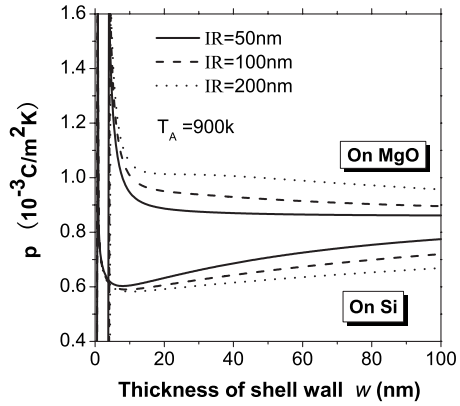

FIG. 2. The electrocaloric coefficient as a function of the wall thickness of nanoshell on MgO and Si core for the various IRs, at room temperature $T=300$ K and annealing temperature $T_A=900$ K.

near the critical nanoshell thickness accompanied with size-driven phase transition. Furthermore, the tensile thermal strain reduces the critical wall thickness where the ferroelectricity disappears, which is totally different from that of the ferroelectric films.[30] According to Eq. (12), it is obvious that

$$\left|Q_{11}\frac{a^2(1-\nu)}{\nu(b^2-a^2)}p'\right| > \left|Q_{12}\left[\frac{2a^2}{b^2-a^2}p' - \frac{u}{b-a}\exp\left(-\frac{R_C}{b-a}\right)\right]\right|, \tag{19}$$

which indicates that the axial thermal strain plays a predomi-

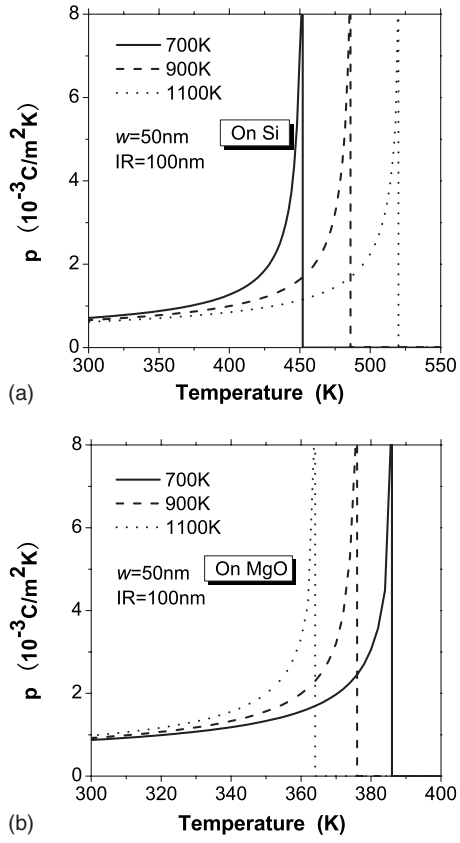

FIG. 3. The electrocaloric coefficient as a function of temperature for the various annealing temperatures under the given IR=100 nm and wall thickness $w=50$ nm; (a) and (b) correspond to Si core and MgO core, respectively.

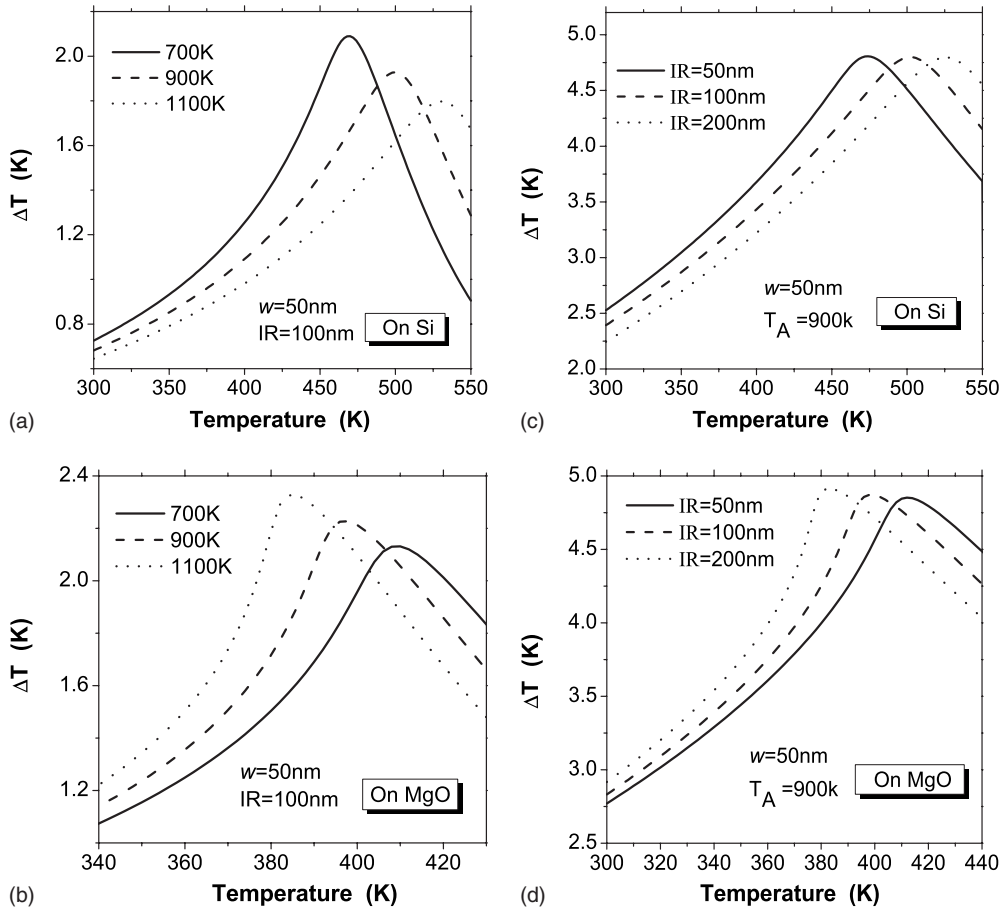

FIG. 4. The temperature dependence of the adiabatic temperature change ΔT under the applied electric field difference $\Delta E = E_2 - E_1$, $E_1 = 10$ kV/cm; (a) and (b) describe the case of different annealing temperatures and fixed IR = 100 nm, $w = 50$ nm, and $\Delta E = 100$ kV/cm; (c) and (d) represent the case of different IRs and given $w = 50$ nm, $T_A = 900$ K, and $\Delta E = 400$ kV/cm.

nant role in influencing the stress field in the nanoshell. Meanwhile, the polarization of nanoshell can be greatly enhanced by the tensile thermal strain and suppressed by the compressive one because of the positive Q_{11}. In the case of the nanoshell on MgO core, the electrocaloric coefficient increases with the increase in IR at a fixed wall thickness. However, the one grown on Si core behaves the opposite way. This can be attributed to the size-dependent stress field in the nanoshell. Apart from shell size, annealing temperature is also an important factor that determines the stress level inside the nanoshell. The electrocaloric coefficient as a function of temperature for the various annealing temperatures is plotted in Figs. 3(a) and 3(b) at IR = 100 nm and wall thickness $w = 50$ nm; (a) and (b) correspond to Si core and MgO core, respectively. The electrocaloric coefficient increases monotonically with temperature and reaches the maximum near the phase transition temperature for a given annealing temperature. It is explained that the abrupt change in the polarization with temperature results in the occurrence of electrocaloric coefficient peak when the temperature is close to the phase transition temperature. In the meantime, the electrocaloric coefficient is dramatically improved near the phase transition temperature, and its corresponding peak also shifts to lower temperature with decreasing annealing temperature in the case of Si core. Nevertheless, the MgO core has an opposite influence on the electrocaloric coefficient. It can be understood that the annealing temperature is responsible for the electrocaloric coefficient by changing the thermal stress level throughout the nanoshell. It should be noted that the tensile thermal strain enhances the polarization along the axial direction through electrostriction and the compressive one has an opposite impact on it, which is different from those in thin films.[25]

Second, the basic principle of reversible and adiabatic ECE is that the tendency of the electric field to reduce the entropy by alignment of electric dipoles has to be compensated by a rise in temperature of the ferroelectric materials. To better understand the effect of the shell size and annealing temperature on the ECE, the temperature dependence of the adiabatic temperature change ΔT for the various annealing temperatures at a given IR = 100 nm and wall thickness $w = 50$ nm is depicted in Figs. 4(a) and 4(b), corresponding to Si core and MgO core, respectively. In order to compare with the results of the bulk sample and thin film $BaTiO_3$, we take the applied electric field difference $\Delta E = E_2 - E_1 = 100$ kV/cm. One can find that the adiabatic temperature change reaches the maximum at an appropriate temperature T_m corresponding to the ferroelectric-paraelectric phase transition temperature. In the case of Si core, the decrease in annealing temperature not only enhances the maximum of adiabatic temperature change to some extent but also decreases T_m. Conversely, the decrease in annealing tempera-

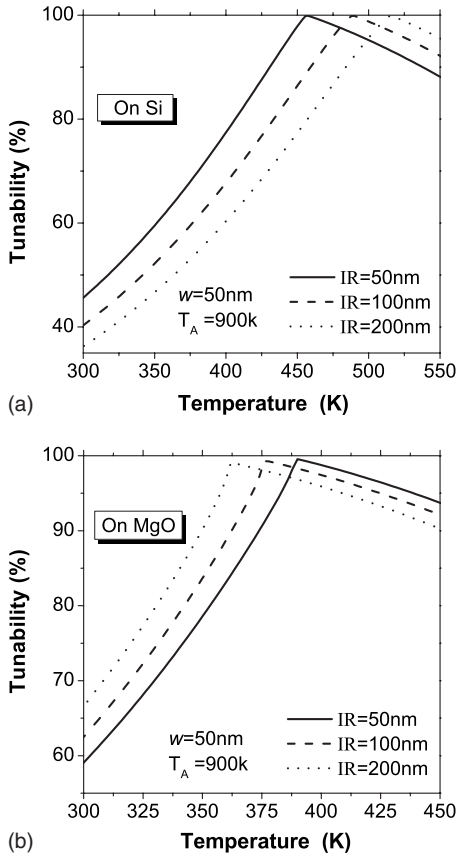

FIG. 5. The dependence of the dielectric tunability on the temperature for the various IRs, at given $w=50$ nm and $T_A=900$ K; (a) and (b) correspond to Si core and MgO core, respectively.

ture shifts the maximal ΔT to higher temperature and reduces its magnitude in the case of MgO core. It is interesting to see that the obvious adiabatic temperature changes $\Delta T(T_m)=2.09$ K at $T_A=700$ K for Si core and $\Delta T(T_m)=2.33$ K at $T_A=1100$ K for MgO core, which are not only much larger than those of bulk $BaTiO_3$ ($\Delta T=1.6$ K) and thin film $BaTiO_3$ ($\Delta T=1.3$ K) (Refs. 24 and 25) but also well consistent with that of dense $BaTiO_3$ nanoceramics ($\Delta T=2.3$ K).[31] The appearance of good ECE can be ascribed to several effects. First, the surface tension of nanoshell differs from the mechanical boundary conditions of single crystal and thin film. Second, the discrepancy of thermal expansion stress levels along the radial and axial directions in the nanoshell have unique influences on the ECE compared with the bulk material and thin film, which has been described along with the electrocaloric coefficient. The adiabatic temperature difference depends on both the extent of electric field change and the initial electric field, which has been systematically investigated by thermodynamic theory.[25] In addition, the temperature dependence of the adiabatic temperature change for the different IRs at $w=50$ nm, $T_A=900$ K, and $\Delta E=E_2-E_1=400$ kV/cm is plotted, as shown in Figs. 4(c) and 4(d). The IR just changes the position of the maximal ΔT, with little influence on the magnitude of maximal ΔT. It is obvious that ECE has been significantly enhanced by higher ΔE, $\Delta T(T_m)=4.81$ K at IR=50 nm for Si core and $\Delta T(T_m)=4.91$ K at IR=200 nm for MgO core.

Finally, the dielectric tunability is numerically calculated by Eqs. (17) and (18), with an applied electric field varying from 0 to 400 kV/cm. Figure 5 displays the temperature dependence of the dielectric tunability for different IRs, at $w=50$ nm and $T_A=900$ K. It is envisaged that the IRs have more impact on the dielectric tunability if the temperature is below the phase transition temperature, and the tunability then reaches the maximum, which is approximately 100% near the phase transition temperature. It can be understood that the small polarization close to the phase transition temperature is more sensitive to the external conditions such as temperature and external electric field; thus small initial polarization would cause large polarization change at certain ΔE, which results in a large dielectric response. Furthermore, the compressive thermal strain can significantly enhance the dielectric tunability under the same IR, wall thickness, and annealing temperature, compared with the influence of tensile thermal strain. The maximal tunability shifts to lower temperature with the decrease in IR in the case of Si core, but it moves to the opposite direction for the nanoshell on MgO core. We conclude that the high dielectric tunability can be achieved by adjusting the IR and by choosing the appropriate core material, which can vary the thermal stress level in the nanoshell. Besides, the radius of the core almost has little effect on the maximum of dielectric tunability.

IV. CONCLUSIONS

In summary, we have investigated the ECE and dielectric response of the $BaTiO_3$ ferroelectric nanoshells within the framework of modified LGD theory. The effects of annealing temperature, wall thickness, and core radius on the electrocaloric coefficient, adiabatic temperature difference, and dielectric tunability are discussed. The calculated results demonstrate that the temperature dependence of ECE is related to both the size of nanoshell and the electric field. The peak of electrocaloric coefficient occurs near the critical nanoshell thickness accompanied with size-driven phase transition. The tensile thermal strain reduces the critical wall thickness where ferroelectricity disappears. This phenomenon is completely different from that of the film. $BaTiO_3$ nanoshell exhibits good ECE with $\Delta T(T_m)=2.09$ K for the nanoshell on Si and $\Delta T(T_m)=2.33$ K for that on MgO, compared with the bulk and thin film $BaTiO_3$ samples. In addition, the compressive thermal strain can significantly enhance the dielectric tunability under the same IR, wall thickness, and annealing temperature compared with the influence of tensile thermal strain. Therefore, ferroelectric nanoshell provides an effective means to acquire enhanced ECE and high dielectric tunability by adjusting the wall thickness, core radius, annealing temperature, and the various core materials, which may open more opportunities for practical application in refrigeration devices.

ACKNOWLEDGMENTS

This work was supported by the National Natural Science Foundation of China under Grant Nos. 10474069 and 50832002, and the Natural Science Foundation of JiangSu Education Committee of China under Grant No. 08KJB140006. One of authors (H.X.C.) was supported by the Jiangsu Government Scholarship for Overseas Studies.

[1]J. F. Scott, Science **315**, 954 (2007).
[2]A. Gruverman and A. Kholkin, Rep. Prog. Phys. **69**, 2443 (2006).
[3]D. D. Fong, G. B. Stephenson, S. K. Streiffer, J. A. Eastman, O. Auciello, P. H. Fuoss, and C. Thompson, Science **304**, 1650 (2004).
[4]W. S. Yun, J. J. Urban, Q. Gu, and H. Park, Nano Lett. **2**, 447 (2002).
[5]Y. Luo, I. Szafraniak, N. D. Zakharov, V. Nagarajan, M. Steinhart, R. B. Wehrspohn, J. H. Wendorff, R. Ramesh, and M. Alexe, Appl. Phys. Lett. **83**, 440 (2003).
[6]M. Alexe, D. Hesse, V. Schmidt, S. Senz, H. J. Fan, M. Zacharias, and U. Gosele, Appl. Phys. Lett. **89**, 172907 (2006).
[7]H. Nonomura, M. Nagata, H. Fujisawa, M. Shimizu, H. Niu, and K. Honda, Appl. Phys. Lett. **86**, 163106 (2005).
[8]X. H. Zhu, P. R. Evans, D. Byrne, A. Schilling, C. Douglas, R. J. Pollard, R. M. Bowman, J. M. Gregg, F. D. Morrison, and J. F. Scott, Appl. Phys. Lett. **89**, 122913 (2006).
[9]M. Alexe, C. Harnagea, D. Hesse, and U. Gösele, Appl. Phys. Lett. **75**, 1793 (1999).
[10]A. N. Morozovska, M. D. Glinchuk, and E. A. Eliseev, Phys. Rev. B **76**, 014102 (2007).
[11]J. E. Spanier, A. M. Kolpak, J. J. Urban, I. Grinberg, L. Ouyang, W. S. Yun, A. M. Rappe, and H. Park, Nano Lett. **6**, 735 (2006).
[12]J. Hong and D. Fang, Appl. Phys. Lett. **92**, 012906 (2008).
[13]J. Junquera and P. Ghosez, Nature (London) **422**, 506 (2003).
[14]Y. Zheng, C. H. Woo, and B. Wang, J. Phys.: Condens. Matter **20**, 135216 (2008).
[15]B. Meyer and D. Vanderbilt, Phys. Rev. B, **63**, 205426 (2001).
[16]I. I. Naumov and H. Fu, Phys. Rev. B **95**, 247602 (2005).
[17]Z. Wang, A. P. Suryavanshi, and M.-F. Yu, Appl. Phys. Lett. **89**, 082903 (2006).
[18]Y. Yang, X. Wang, C. Zhong, C. Sun, and L. Li, Appl. Phys. Lett. **92**, 122907 (2008).
[19]Z. Dang, D. Xie, and C. Shi, Appl. Phys. Lett. **91**, 222902 (2007).
[20]A. S. Mischenko, Q. Zhang, J. F. Scott, R. W. Whatmore, and N. D. Mathur, Science **311**, 1270 (2006).
[21]A. S. Mischenko, Q. Zhang, J. F. Scott, R. W. Whatmore, and N. D. Mathur, Appl. Phys. Lett. **89**, 242912 (2006).
[22]B. Neese, B. Chu, S.-G. Lu, Y. Wang, E. Furman, and Q. M. Zhang, Science **321**, 821 (2008).
[23]J. Hagberg, A. Uusimaki, and H. Jantunen, Appl. Phys. Lett. **92**, 132909 (2008).
[24]G. Akcay, S. P. Alpay, J. V. Mantese, and G. A. Rossetti, Jr., Appl. Phys. Lett. **90**, 252909 (2007).
[25]G. Akcay, S. P. Alpay, G. A. Rossetti, Jr., and J. F. Scott, J. Appl. Phys. **103**, 024104 (2008).
[26]L. J. Dunne, M. Valant, G. Manos, A.-K. Axelsson, and N. Alford, Appl. Phys. Lett. **93**, 122906 (2008).
[27]S. Prosandeev, I. Ponomareva, and L. Bellaiche, Phys. Rev. B **78**, 052103 (2008).
[28]A. N. Morozovska, M. D. Glinchuk, and E. A. Eliseev, Phase Transitions **80**, 71 (2007).
[29]S. P. Timoshenko and J. N. Gooier, *Theory of Elasticity* (McGraw-Hill, New York, 1970).
[30]M. B. Okatan, M. W. Cole, and S. P. Alpay, J. Appl. Phys. **104**, 104107 (2008).
[31]J. H. Qiu and Q. Jiang, J. Appl. Phys. **105**, 034110 (2009).